The solar thermal treatment of manganese ore pellets using closed-loop forced convection of air

Cite as: AIP Conference Proceedings **2126**, 150003 (2019); https://doi.org/10.1063/1.5117659
Published Online: 26 July 2019

Lina Hockaday, Frank Dinter, Thomas Harms, and Quinn Reynolds

The Solar Thermal Treatment of Manganese Ore Pellets Using Closed-Loop Forced Convection of Air

Lina Hockaday[1, 2 a)], Frank Dinter[2], Thomas Harms[3] and Quinn Reynolds[1)]

[1] *MINTEK. Address: Private Bag X3015, Randburg 2191, South Africa.*
[2] *Solar Thermal Energy Research Group (STERG), Mechanical Engineering Building, Joubert Street, Stellenbosch 7600, South Africa.*
[3] *Department of Mechanical and Mechatronic Engineering, University of Stellenbosch, Joubert Street, Stellenbosch 7600, South Africa.*

[a)] Corresponding author: linah@mintek.co.za

Abstract. The incorporation of renewable energy sources in high temperature industrial processes has the potential to reduce energy costs as well as greenhouse gas emissions. The current study forms part of an evaluation of the opportunities to integrate concentrating solar thermal energy into the sintering of manganese ores. The study includes the results of direct irradiation of manganese ore pellets with concentrating solar flux in combination with the closed-loop forced convection of air. The results of this study will be of interest to the fields of high temperature solar thermal process heat and solar thermal materials processing as well as manganese ore sinter production.

INTRODUCTION

The thermal treatment of manganese ores for preheating and prereduction has been extensively investigated as part of sinter production from ore fines [1]. The current state of the art technology relies on diesel and coal combustion heating to produce sinter that is suitable as feed for both blast furnaces and submerged electric arc furnaces (SAFs) [2]. SAFs produce ferro-manganese alloys that are added to steel to improve properties such as toughness and wear resistance [3]. Due to increasing pressure to reduce the carbon footprint of steel production and growing concern and legislation regarding the emission of greenhouse gasses, the concept of thermal treatment of manganese ores using concentrating solar thermal energy is being investigated [4]. The aim of the current experiments is to advance the concept of a solar sinter process through the investigation of the multi-mode heat transfer through a packed bed of manganese ore pellets. Initial tests on direct solar irradiation of manganese ores and manganese ore pellets showed that conduction through the ore pellets is insufficient to evenly heat a sample with a depth of 50 mm [5]. This was confirmed by tests conducted on single pellets by Prof. Flamant [6]. The tests used a parabolic reflector with a diameter of 1.5 m and a focus of 10 mm to heat individual manganese ore pellets with concentrating solar radiation. One such pellet is shown in Fig. 1. Although the pellet melted on the side exposed to the radiation, indicating temperatures well above 1200 °C, the thermocouple inside the pellet only reached a temperature of 950 °C, well below the target sinter temperature of 1200 °C. When commercial sinter belts treat layers of sinter that are up to 600 mm thick, it is clear that heat transfer of solar thermal energy through the samples needs to be enhanced if it is to be seen as a viable alternative. This paper will detail the improved results when using a closed air loop with forced convection to increase heat transfer through a 50 mm deep sample of manganese ore pellets, as well as the estimation of heat transfer coefficients and a thermodynamic model to describe the observed behavior of the manganese ore pellets.

SolarPACES 2018
AIP Conf. Proc. 2126, 150003-1–150003-10; https://doi.org/10.1063/1.5117659
Published by AIP Publishing. 978-0-7354-1866-0/$30.00

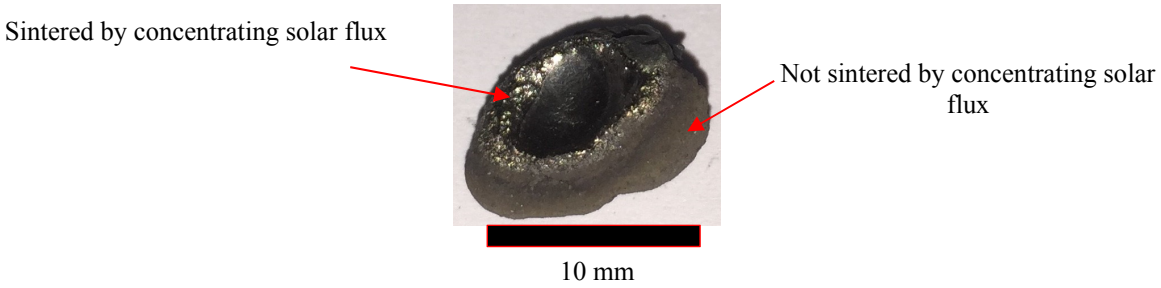

FIGURE 1. Picture of manganese ore pellet irradiated by concentrating solar flux

EXPERIMENTAL SET-UP

Solar heat treatment of the pellets prepared from Mamatwan manganese ores [7] were conducted at the University of Stellenbosch rooftop solar facilities in South Africa during April 2018. The concentrator used was a two-axis tracking solar dish built by flat mirrors as shown in Fig. 2(a). The receiver design, Fig. 2(b) included a small stainless steel fan driven by a DC motor to circulate air in a closed loop through the irradiated sample. K-type thermocouples were used to measure the air temperatures at the front and back of the sample. A pitot tube connected to pressure transducers was used to measure the air velocity in the closed loop. Data was logged electronically every 30 seconds. Each sample was irradiated for 60 minutes.

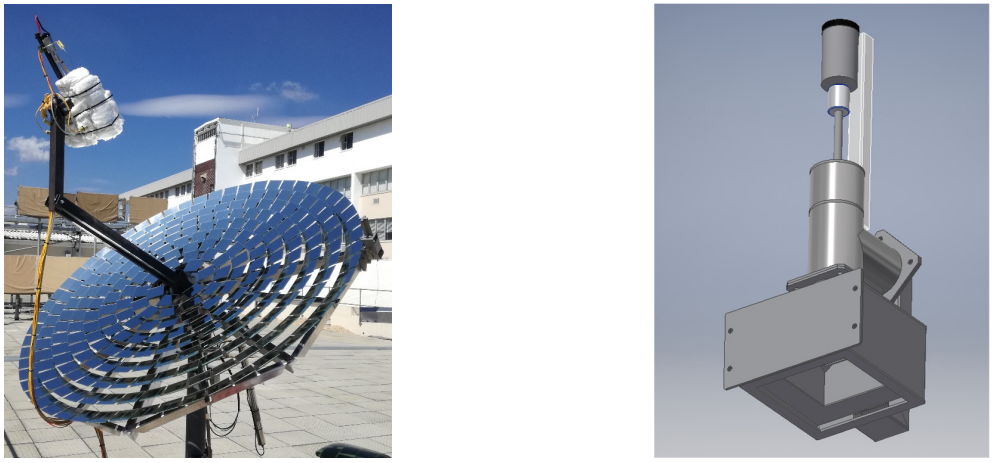

(a) (b)

FIGURE 2. Experimental set-up (a) and (b) sketch of the receiver with closed air loop. Sketch (b) published with permission from Hein Joubert, STERG.

The manganese ore pellets were made from manganese ore from the Kalahari Manganese Field deposit in South Africa. The ore was pulverised and mixed with water and 3 % bentonite binder and then spinned on a disk to create pellets. This method is identical to the preparation of manganese ore pellets used in for previous results obtained with no forced convection, as described for SolarPACES 2017 [5]. The manganese ore pellets used were of the size fraction 100 % passing through 13 mm sieve apertures and 0 % passing 6 mm sieve apertures. The samples were contained in small cages made from stainless steel mesh with a square face of 90 mm x 90 mm towards the incoming air flow and solar flux. The depth of the cage was 50 mm.

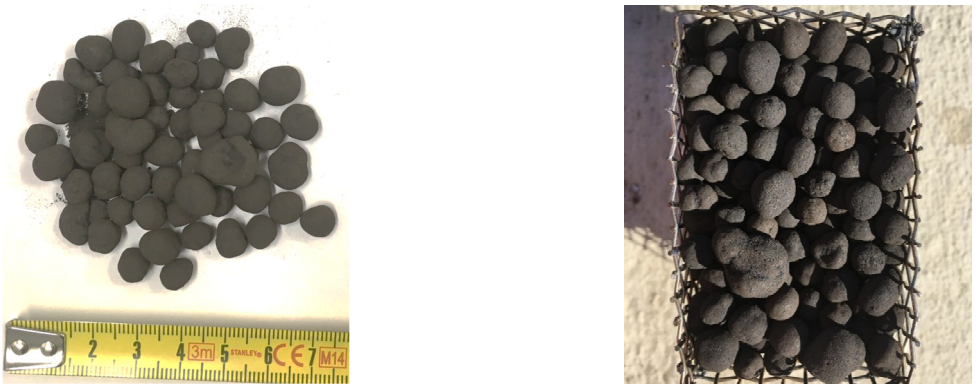

(a) (b)

FIGURE 3. Untreated (a) and treated (b) manganese ore pellets

RESULTS

Measurements

The positions where temperatures were measures are shown below in Fig. 4(a).

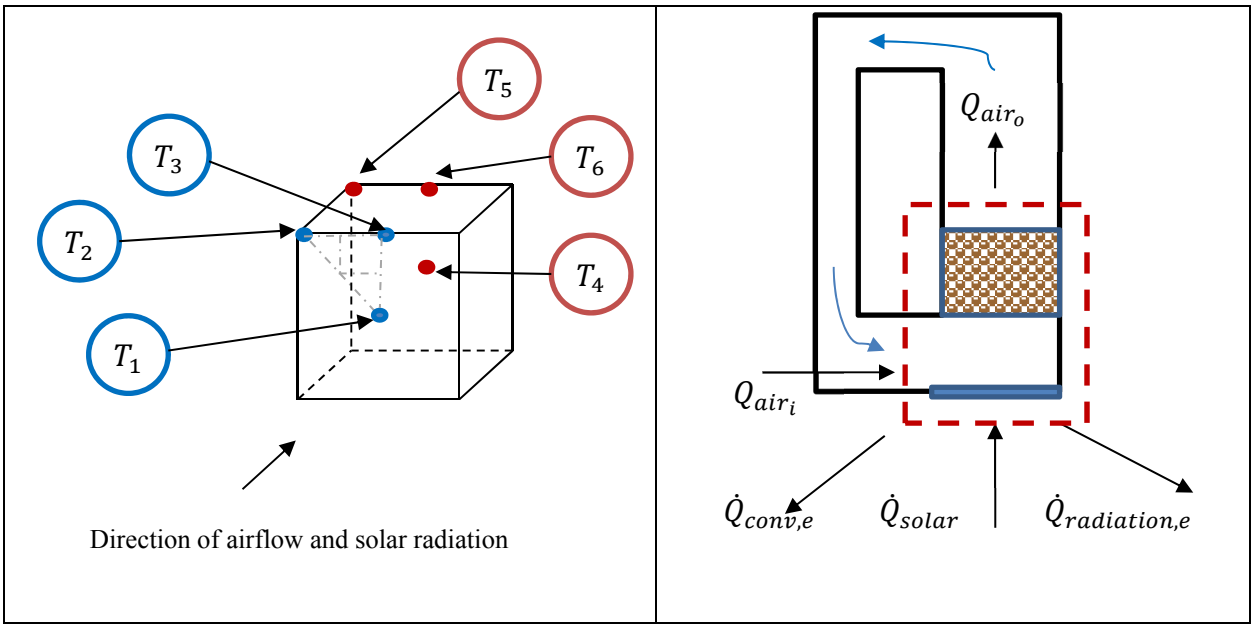

(a) (b)

FIGURE 4. (a) Position of temperature measurements with T_1, T_2 and T_3 on the air inlet side and with T_4, T_5 and T_6 on the air outlet side and (b) an energy balance over the receiver and packed bed.

In order to assess the thermal treatment of the pellets, some average temperatures were defined as follow. T_i is used as the average air inlet temperature of the air to the bed while T_o is the average outlet temperature of the air from the bed. The average inlet and outlet temperature is based on geometry described by grey dash-dot lines in Fig. 4(a). T_b is the average air temperature through the bed. We also define T_s as the average surface temperature of the pellets.

$$T_i = \frac{T_1}{4} + \frac{T_2}{4} + \frac{T_3}{2} \quad (1)$$

$$T_o = \frac{T_4}{4} + \frac{T_5}{4} + \frac{T_6}{2} \quad (2)$$

$$T_b = \frac{T_i + T_o}{2} \quad (3)$$

The experimental results show improvement in both the increased average temperatures achieved on the cold side of the sample and a decrease in the thermal gradients observed across the sample. The sample temperatures on the cold side improved from measurements in a range of 350 °C to 580 °C without forced convection to measurements in a range of 630 °C to 690 °C with forced convection and this is illustrated by plots of T_b against time as shown in Fig. 5 as well as plots of the temperature difference measured over the bed, $T_i - T_o$ as shown in Fig. 6.

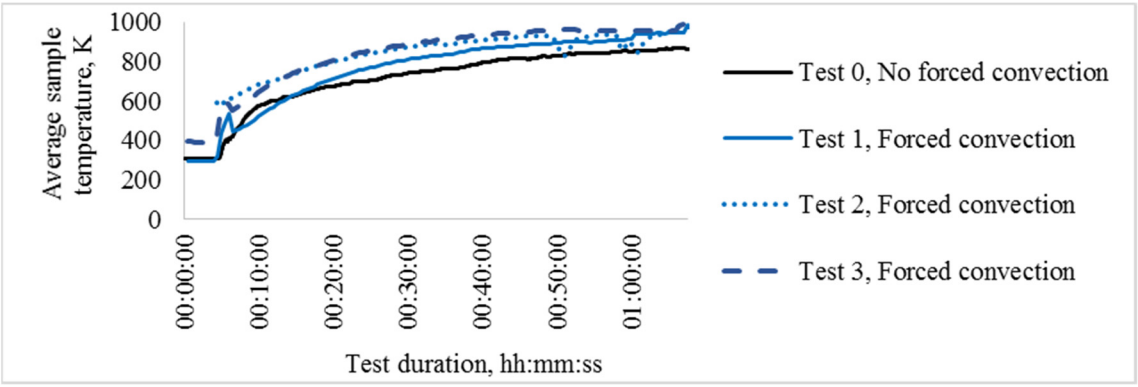

FIGURE 5. Average sample temperatures, T_b, for tests without and with forced convection

Test 2 was influenced by cloud cover towards the end of the experiment. The observed temperature gradient measured across the sample decreased from 300 °C without forced convection to a 150 °C at the end of the forced convection experiments as illustrated in Fig. 6.

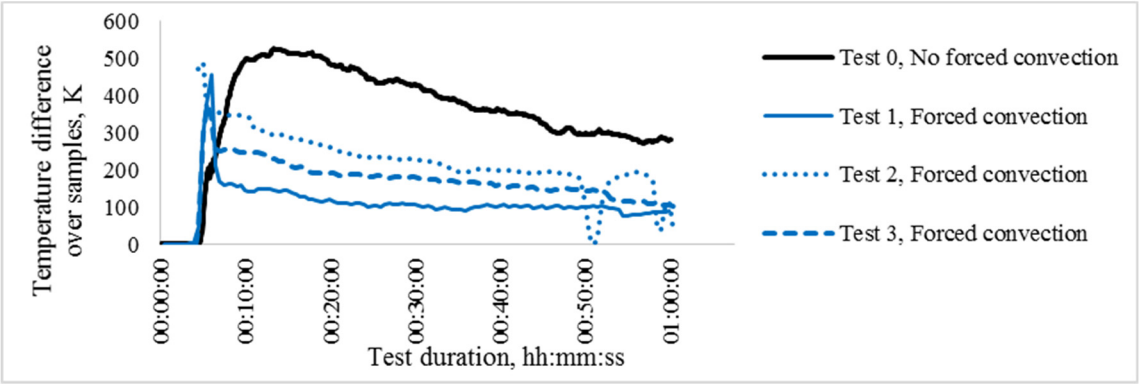

FIGURE 6. Average temperature difference across sample bed, $T_i - T_o$.

The heat transfer through the sample was treated as a packed bed and heat transfer coefficients were obtained for varying air velocities measured in the closed loop. The air velocity in the closed loop was calculated from measurements for the static and stagnation pressures by a pitot tube with pressure transducers according to equation 4 [8].

$$u \approx \left[2\frac{p_0 - p_s}{\rho}\right]^{1/2} \quad (4)$$

, where, u is the midstream velocity (m/s), p_o is the static pressure (Pa), p_s is the stagnation pressure (Pa) and ρ is the air density (kg/m^3)

As the air properties are dependent on temperature, the appropriate density, viscosity, specific heat and thermal conductivity values for the measured air temperatures were determined form published data [9]. Due to the rectangular geometry and variance observed in the pressure measurements, turbulent flow is assumed in the closed air loop. Velocity profiles in rectangular ducts [10] indicate that the average velocity is significantly lower than the measured midstream velocity in the duct even for turbulent conditions. As the velocity profile for the rectangular duct has not been determined yet, the measured velocity, u, was multiplied by 0.75 to estimate the average air velocity, u^*, in the closed air loop. The pressure measurements were corrected for gain and drift observed due to heating of the pressure transducers. The superficial velocity over the packed bed of particles can now be calculated by applying the law of mass conservation on the air stream at cross-sectional areas 1 and 2 as indicated in Fig. 7.

$$\dot{m}_1 = \dot{m}_2 = u_1^* \cdot A_1 \cdot \rho_1 = u_2^* \cdot A_2 \cdot \rho_2 \quad (5)$$

$u_2^* = \frac{u_1^* A_1 \rho_1}{A_2 \rho_2}$, where subscripts indicates position in the set-up as per Fig. 7. A is the cross sectional area in m^2. μ is the air viscosity in (Pa.s) (6)

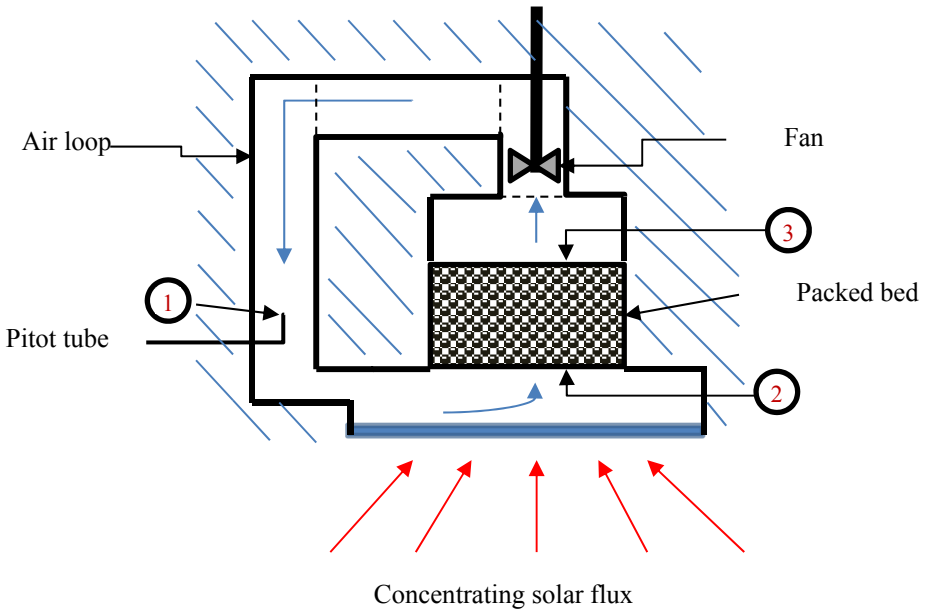

FIGURE 7. Sketch for solar treatment with forced air loop heat transfer

Heat Transfer

Neglecting any reactions, an energy balance over the system can now be described as below and in Fig. 4(b).

$$\dot{Q}_{solar} + \dot{Q}_{air_i} - \dot{Q}_{air_o} - \dot{Q}_{conv,e} - \dot{Q}_{radiation,e} = \dot{Q}_{cond,b} + \dot{Q}_{conv,b} \quad (7)$$

$$\dot{Q}_{solar} = \eta q_0 \mathrm{A} \quad (8)$$

$$\dot{Q}_{air,i} - \dot{Q}_{air,o} = \dot{m} \int_{T_{,o}}^{T_7} C_p \, dT \quad (9)$$

$$\dot{Q}_{conv,e} = hA(T_i - T_A) \quad (10)$$

$$\dot{Q}_{radiation,e} = \varepsilon\sigma A(T_i^4 - T_A^4) \quad (11)$$

$$\dot{Q}_{cond} = -k_p A\partial T/\partial x \quad (12)$$

$\dot{Q}_b$ is given by equation 21to follow.

The average air velocity is used to determine the Reynolds number for flow through a packed bed as described by Whitaker [11] in equation 13. The heat transfer through the packed bed of manganese ore pellets was evaluated for three time periods where the measured air velocity and temperatures measured around the bed were approaching steady state. The sample was treated as a packed bed and the heat transfer coefficients were determined based on the evaluation of the heat transfer correlation expressing the Nusselt number (N_{Nu}) as a function of the Reynolds number (N_{Re}), see equation 19, also expressed for packed beds [11]. The dimensionless numbers were defined as follow:

$N_{Re} = \frac{u_b L^* \rho}{\mu}$, where ρ is the air density (kg/m^3). (13)

$$N_{Nu} = \frac{h_{lm} L^*}{k} \quad (14)$$

The characteristic air velocity, u_b, and the characteristic length, L^*, are defined as:

$u_b = \frac{u_2^*}{\epsilon A_2}$, the air velocity through the voids in the bed (15)

$L^* = D_p(\frac{\epsilon}{1-\epsilon})$, characteristic length (m) (16)

The void fraction, determined experimentally, is given in equation 17. The void fraction was determined by filling a measuring cylinder to a known volume with pellets and measuring the volume of water that can be added to that volume. As a first approximation the particles are assumed to be spherical with a diameter, D_p.

ϵ = (Void volume)/(Total bed volume) = 0.49 (17)

$$D_p = 0.010 \text{ m} \quad (18)$$

The heat transfer correlation is given as:

$$N_{Nu} = \left(0.5N_{Re}^{\frac{1}{2}} + 0.2N_{Re}^{\frac{2}{3}}\right) N_{Pr}^{\frac{1}{3}} \quad (19)$$

With $N_{Pr} = \frac{C_p \mu}{k} = 0.7$ for air over the applicable temperature range and where C_p is the specific heat at constant pressure ($\frac{J}{kg \cdot K}$)and k is the thermal conductivity of air ($\frac{\text{W}}{\text{m}^2 \cdot \text{K}}$). (20)

For each time period considered, the Reynolds number was calculated using densities and viscosities for the average bed temperature, T_b, calculated for that time period. The Reynolds number was then used with equation 19 to find the Nusselt number. Equation 14 was re-arranged to obtain the heat transfer coefficient, h_{lm}. With the heat transfer coefficient known, we are able to estimate the heat transfer rate to the packed bed, Q_b.

$\dot{Q}_b = h_{lm} a_b V_b \Delta T_{lm}$, where a_b is the pellet surface area per unit volume and V is the total volume of the packed bed, and ΔT_{lm} is the log-mean temperature difference (21)

$\Delta T_{lm} = \frac{T_o - T_i}{\ln\left(\frac{T_S - T_i}{T_S - T_o}\right)}$, where T_s is the surface temperature of the pellets and all temperatures in K. (22)

The surface temperature of the pellets was measured by T_5 which was in direct contact with the pellets and showed least response from step changes in solar flux and air velocity conditions as it was shielded from radiation by the bed and shielded from convection due to boundary layer effects at the wall. The temperature measurements and calculated velocities used for the heat transfer analysis is shown in Fig. 8.

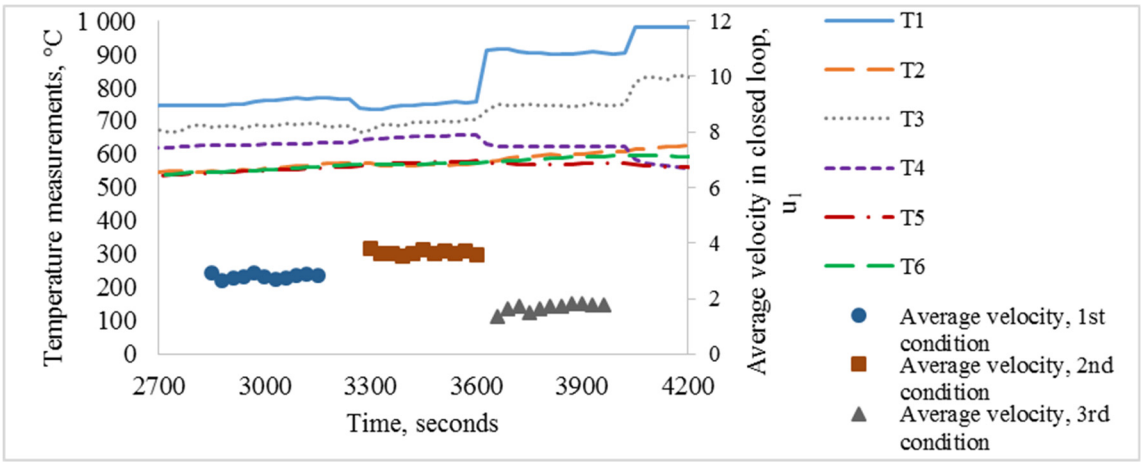

FIGURE 8. Test 1 temperature measurements (lines, left y-axis) and air velocity (markers, right y-axis) data for heat transfer analysis

The convective heat transfer, $\dot{Q}_b$, can now be compared to the conductive heat transfer, $\dot{Q}_{cond}$, using equation 23 and the effective thermal conductivity of the pellets, k_p , previously determined as 0.658 $\frac{W}{m \cdot K}$ [5] and the area, A, and distance over the bed, x ., as given by the bed geometry.

$$\dot{Q}_{cond} = -k_p A \partial T / \partial x \quad (23)$$

The results from this analysis are tabulated in TABLE 1.

TABLE 1. Table with results from heat transfer analysis for Test 1, April 2018

Period, (s)	Duration, (s)	u_b, (m/s)	N_{Re}	N_{Nu}	h_{lm},$\left(\frac{W}{m^2 \cdot K}\right)$	$\dot{Q}_b$, (W)	$\dot{Q}_{cond}$, (W)
2850-3150	300	134	12694	147	957	-6749	-11
3300-3600	300	170	15648	167	1100	-6616	-9
3660-3960	300	87	7510	107	728	-6582	-17

$\dot{Q}_b$ is negative indicating that energy is lost by the air stream and gained by the packed bed. This analyses can be improved by including the reactions indicated by the mineralogy results, but this is outside the current scope of work.

Mineralogy

The mineralogy of the sample is important as any preheated, pretreated or sintered manganese ore needs to be of a quality suited to be fed into a SAF or blast furnace. The paper also reports on differences in the mineralogy of the untreated and irradiated pellets to serve as confirmation of the pellet temperature achieved at the air temperatures measured. The mineralogy will be discussed based on thermogravimetric experiments of the ores and mineralogical assays. The mineralogical assays include scanning electron microscopy (SEM) of sections through selected pellets.

The SEM image of an untreated or green pellet, Fig. 9(a), shows that the pellets are an agglomeration of dense minerals with sharp edges and banded as well as speckled intergrowth. In the SEM images voids are black, silica rich minerals and calcium rich minerals are dark in color and manganese rich minerals are light in color. The images of solar heat treated pellets, Fig. 9(b) and Fig. 10(a), shows small voids forming inside the pellets indicating that thermal decomposition and calcination reactions did occur, resulting in gasses being released from the minerals. The rounding of silica rich particles indicate melting of these mineral phases did occur and in general mineral particles developed jagged borders indicating that softening of these minerals have started to occur.

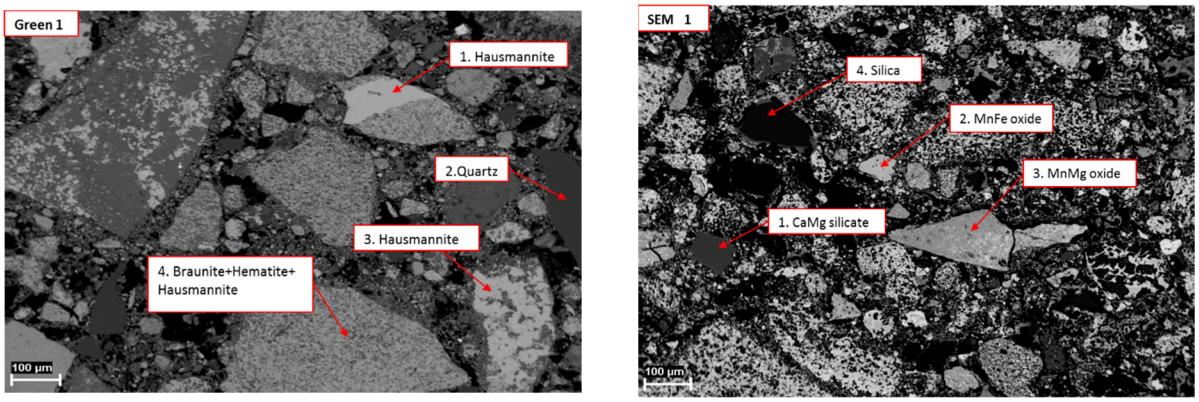

(a) (b)

FIGURE 9. SEM images for manganese pellets before (a) and after (b) treatment

For comparison, we include a SEM image of a particle treated at CNRS-PROMES [6] in Fig. 10(b). The surface has completed agglomerated and no individual particles are visible indicating complete sintering of the pellet surface. The pellet still shows a highly porous structure, which is desirable for smelting in SAFs. This is confirmation that carbon is not necessary for sinter production if an alternative heat source is supplied.

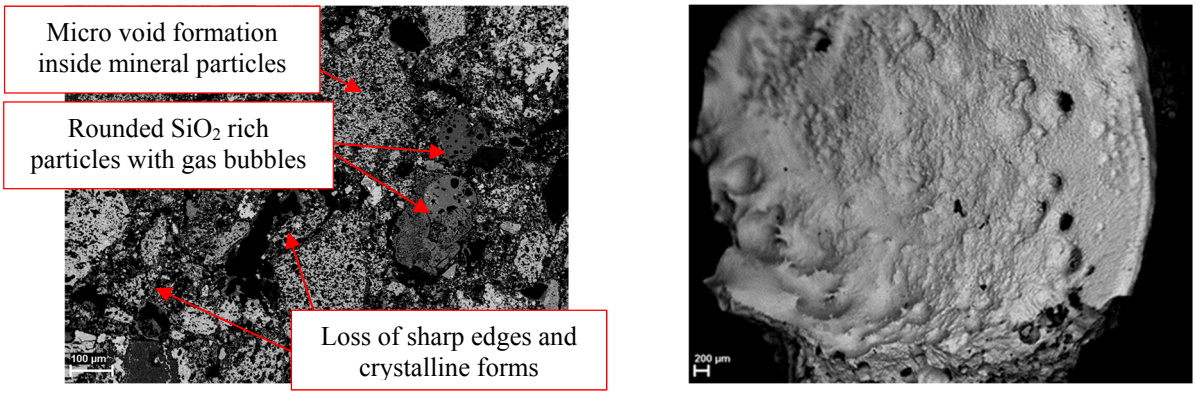

(a) (b)

FIGURE 10. Morphology changes in manganese ore samples after solar treatment (a) and SEM image of manganese ore pellet partially sintered at CNRS-PROMES [6] (b)

Thermodynamics

Results from the bulk chemical analysis and mineralogy of the ores were used to inform equilibrium models using FactSage 7.0 thermodynamic software [12]. The software uses minimization of the Gibbs free energy to determine the equilibrium of phases at different temperatures and predicts the trends of manganese ores during reduction [7] and smelting [13]. Since the thermodynamic database does not include data on all the mineralogical compounds in manganese ores, the ores were approximated by simplifying the mineralogy as shown in Table 2. Where possible, the simplified model conserved the valences of manganese and iron.

TABLE 2. Composition of sample as used for equilibrium model

Fe_2O_3	Mn_3O_4	MnO	SiO_2	$CaCO_3$	$FeCO_3$	$MgCO_3$	$MnCO_3$	Mn_2O_3	MnO_2	H_2O	K_2O	C	Total
3.5	7.3	3.8	6.9	28.0	3.7	2.9	0.4	27.1	9.9	0.5	1.1	5	100

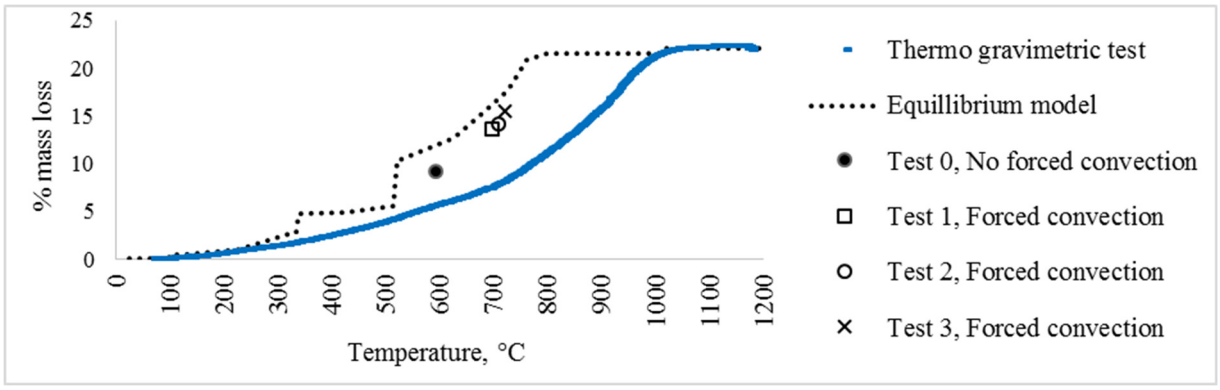

FIGURE 11. Thermo gravimetric experimental mass loss as compared to FACTSage model and on sun test results. Mass loss for experiments are plotted with the maximum bed temperature, T_b, calculated for each experiment.

The thermo-gravimetric (TG) data was collected for a heating rate of 10 °C/min until 1200 ° was reached. This temperature was maintained until no further mass loss was observed. Comparing the TG data with the equilibrium model, the total mass loss at 1200 °C is in agreement. However, the TG data shows mass losses less than the predicted equilibrium, indicating that the sample did not reach equilibrium at each temperature. The experiments under solar radiation did not reach 1200 °C, but maintained the maximum bed temperature for a sufficient time to achieve results closer to the equilibrium prediction. Both the heat transfer model and the thermodynamic model will be used to extrapolate to the case of a pilot scale solar sinter belt in future work to address the technical challenges and feasibility of scaling up the concept. Using Fig.12 in conjunction with Fig. 11, we can estimate that the average temperature of the pellets were increased from 600 °C to 700 °C by using forced convection. This relates to an increased energy transfer to the pellets from 0.89 MJ/kg to 1.18 MJ/kg. If this solar thermal energy were to replace carbon combustion as heat source [14] in a sinter plant, the carbon saving would increase from 34 g carbon/kg sinter for no convection to 45 g carbon/ kg sinter with forced convection. Realizing that currently sinter production uses 100 g carbon/ kg sinter [1] partial replacement of this carbon with solar thermal energy for heating up to 700 °C could potentially reduce greenhouse gas emissions at sinter plants by 45 %.

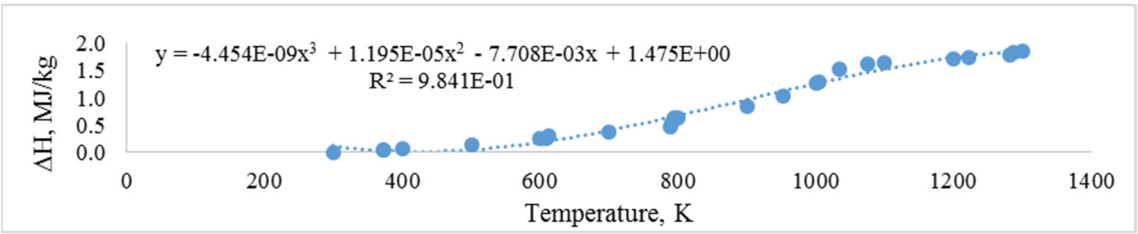

FIGURE 12. Energy requirements as determined by equilibrium model (FACTSage)

CONCLUSION

The pretreatment of manganese ores with concentrating solar thermal energy can potentially reduce CO_2 emissions compared to traditional pretreatment technologies [2], but heat transfer of solar thermal energy needs to be enhanced to achieve results comparable to the current state of the art sinter technology. Adding closed-loop forced convection to the experimental setup improved the heat transfer through the sample and reduced the thermal gradient over the sample significantly. This increases the viability of the solar sinter concept by proving that solar energy can be used to achieve even heating of a packed bed with low thermal conductivity when force convection is employed to improve heat transfer.

ACKNOWLEDGMENTS

This paper is published by permission of Mintek. Our thanks to the Mineralogy Division at Mintek for the SEM images and mineral identification. The authors would also like to thank Stellenbosch University and the Solar Thermal Energy Research Group (STERG) for the use of their concentrator and assistance in running the experiments, particularly JC Nel and Hein Joubert. Our thanks to Transalloys Pty. Ltd. for donating the manganese ore samples for testing. We acknowledge the funding support of the Centre for Renewable and Sustainable Energy Studies (CRSES) that allowed conference attendance. The authors would also like to thank Prof. Gilles Flamant from the CNRS-PROMES for the feasibility tests conducted on our behalf.

REFERENCES

1. P.C. Pienaar and W.F.P. Smith, "A case study of the production of high-grade manganese sinter from low-grade Mamatwan manganese ore," Proceedings of the 6th International Ferroalloys Congress, Volume 1 (SAIMM, Cape Town, South Africa, 1992), pp 131–138.
2. S.A.C. Hockaday, F.Dinter, and T.M. Harms, "Introducing solar thermal heat into minerals processing: A case study on replacing a diesel burner at a sinter plant." *Conference Proceedings: 5th Southern African Solar Energy Conference*, (SASEC 2018, Durban, South Africa, 2018), [online] Available at https://www.sasec.org.za/full_papers/74.pdf [Accessed 28 August 2019].
3. Sverre E. Olsen, Merete Tangstad, and Tor Lindstad, "Alloy specification and uses," in *Production of Manganese Ferroalloys*, (Tapir academic press, Trondheim, 2007), pp. 15-18.
4. M. Lubkoll, S.A.C. Hockaday, T.M. Harms, and T.W. von Backstrom, "Integrating solar process heat into manganese ore pre-heating," In *Conference Proceedings: 5th Southern African Solar Energy Conference*, (SASEC 2018, Durban, South Africa, 2018). [online] Available at https://www.sasec.org.za/full_papers/57.pdf [Accessed 28 August 2019].
5. S.A.C. Hockaday, F. Dinter, T.M. Harms, and Q.G. Reynolds, "Solar thermal treatment of manganese ore fines," In *Proceedings of SolarPACES 2017*. API Conference Proceedings 2033, 140001 (American Institute of Physics, Melville, NY, 2018), pp. 1-10.
6. Gilles Flamant (private communication).
7. Bjorn Sorensen, Sean Gaal, Eli Ringdalen, Merete Tangstad, Ring Kononov, and Oleg Ostrovski, "Phase compositions of manganese ores and their change in the process of calcination," in *International Journal of Mineral Processing* 94, Issues 3-4, (Elserivier, 2010), pp.101-110.
8. Frank M. White. "Viscous flow in Ducts," in *Fluid Mechanics*, Fifth Edition. (McGraw-Hill, 2003), pp. 407.
9. Peter E. Liley, George H. Thomson, D.G. Friend, Thomas E. Daubert, and Evan Buck, "Physical and Chemical Data," in *Perry's Chemical Engineers' Handbook,* edited by Robert H. Perry, (McGraw, 1997), pp. 208-209.
10. Lawrence C. Hoagland "Fully developed turbulent flow in straight rectangular tubes," PhD thesis, Department of Mechanical Engineering, Massachusetts Institute of Technology, 1960.
11. Stephen Whitaker, "Forced convection heat transfer correlations for flow in pipes, past flat plates, single cylinders, single spheres, and for flow in packed beds and tube bundles," in *AIChE Journal*, 18(2), (1972), pp. 361 – 371.
12. C.W. Bale, E. Bélisle, P. Chartrand, S.A. Decterov, G. Eriksson, K. Hack, I.-H. Jung, Y.-B. Kang, J. Melançon, A.D. Pelton, C. Robelin, and S. Petersen "FactSage thermochemical software and databases: Recent developments," *Calphad 33(2),* (Elsevier Science Ltd, 2009*), pp.* 295–311.
13. Eli Ringdalen, Sean Gaal, Merete Tangstad, and Oleg Ostrovski, "Ore melting and reduction in silicomanganese production," *Metallurgical and Materials Transactions B,41(6),* (Springer US, 2010), pp. 1220-1229.
14. Engineering Toolbox, "Fuels - higher and lower calorific values," 2003. [online] Available at : https://www.engineeringtoolbox.com/fuels-higher-calorific-values-d_169.html [Accessed 28 August 2019].